Electronic Supplementary Information

Colloidal CdS and CdZnS nanocrystal photocatalysts with massive S^{2-}-adsorption: one-step facile synthesis and highly efficient H_2-evolution performance

Wei Zhong,[a] Ying Huang,[b] Xuefei Wang,[b] Jiajie Fan[c] and Huogen Yu*[ab]

[a] State Key Laboratory of Silicate Materials for Architectures, Wuhan University of Technology, Wuhan 430070, PR China

[b] Department of Chemistry, School of Chemistry, Chemical Engineering and Life Sciences, Wuhan University of Technology, Wuhan 430070, PR China

[c] School of Materials Science and Engineering, Zhengzhou University, Zhengzhou 450002, PR China

Tel: 0086-27-87756662, Fax: 0086-27-87879468

E-mail: yuhuogen@whut.edu.cn (H.Yu)

Part I: Experimental details

1.1 Synthesis and photocatalytic H_2-generation tests of colloidal CdS-NCs

The colloidal CdS-NC photocatalyst was synthesized via a facile precipitation method in a sulfur-rich system (a 0.35 M Na_2S/ 0.25 M Na_2SO_3 mixing solution). Typically, 1.15 mL of $Cd(NO_3)_2$ solution was quickly added into 80 mL of mixing solution with 0.35 mol/L Na_2S and 0.25 mol/L Na_2SO_3 under vigorously stirring. After maintain for another 60 min, a yellow solution was obtained. In this case, the ratio of Cd^{2+} to S^{2-} was designed to be ca. 1:810, and the amount of CdS-NC photacatalyst was controlled to be 5 mg. To characterize the morphology and microstructures via FESEM and TEM, the CdS-NCs were collected by centrifugation, washed with distilled water several times, and finally dispersed in ethanol by ultrasound. For the CdS-NC powder, the above colloidal CdS-NC solution was centrifuged and washed with distilled water several times and then dried at 60 °C for 12 h. For the photocatalytic H_2-evolution test of colloidal CdS-NCs, the above colloidal CdS-NC solution was directly used for the following H_2-evolution reaction after purged with N_2 for 15 min. A 350-W Xe lamp with a UV cutoff filter ($\lambda \geq 420$ nm) was used as the light source, and the amount of evolved H_2 was tested using a Shimadzu gas chromatograph (a thermal conductivity detector and a 5 Å molecular sieve column, Shimadzu GC-2014C, Japan).

1.2 Synthesis and photocatalytic H_2-evolution experiments of *c*-CdS and *h*-CdS

The *h*-CdS photocatalyst was synthesized via a typical precipitation-calcination rout. Briefly, a Na_2S solution (0.1 mol L^{-1}, 250 mL) was added into $Cd(NO_3)_2$ solution (0.1 mol L^{-1}, 250 mL) under stirring, and finally orange precipitates were obtained. After stirring for another 4 h, the suspension was aging for 24 h. The precipitate was filtered, washed with water and ethanol several times, followed by dried at 60 °C for 24 h. After grinded into powder, the obtained orange product was labeled as *c*-CdS. Next, the above *c*-CdS was calcined at 550 °C for 4 h under N_2 atmosphere to prepare traditional hexagonal CdS (*h*-CdS). As for the photocatalytic H_2-generation tests of *c*-CdS and *h*-CdS, their corresponding power (50 mg) was dispersed in the sulfur-rich solution (80 mL, 0.25 M Na_2SO_3 and 0.35 M Na_2S), and the following process is similar to that of colloidal CdS-NCs. The as-obtained *c*-CdS and *h*-CdS powder were used for its corresponding characterization.

1.3 Synthesis and photocatalytic H_2-production experiments of colloidal CdZnS-NCs

The colloidal CdZnS-NCs were prepared by a one-step co-precipitation strategy in a sulfur-rich system, similar to the above synthesis of colloidal CdS-NCs. In a typical synthesis, 114.7 μL of 0.044 mol L^{-1} $Zn(NO_3)_2$ solution was added into 116.2 μL of 0.03 mol L^{-1} $Cd(NO_3)_2$ solution to form a Zn/Cd mixing solution. Then, the above Zn/Cd mixing solution was directly poured into 80 mL of the sulfur-rich system under vigorously stirring. After stirred for 60 min, a colloidal $Cd_{0.4}Zn_{0.6}S$-NC solution containing 1 mg photocatalyst was obtained. Additionally, various colloidal $Cd_xZn_{1-x}S$-NCs (x = 1, 0.8, 0.6, 0.4, 0.2, 0) were also prepared by changing the volume ratio

of $Cd(NO_3)_2$ to $Zn(NO_3)_2$ solution with aim of investigating the relation between the bandgap structure and photocatalytic H_2-evolution activity. As for the characterization and photocatalytic H_2-evolution test of colloidal CdZnS-NCs, the process is similar to the colloidal CdS-NCs, and the detailed experiments can be referred in **1.1 Synthesis and photocatalytic H_2-generation tests of colloidal CdS-NCs**.

1.4 Characterization

X-ray diffraction (XRD) data was obtained by a Rigaku III X-ray diffractometer. The morphology and structure of various samples was recorded by a JSM-7500F field emission scanning electron microscope (FESEM) and JEM-2100F transmission electron microscope (TEM) acquired with an energy dispersive X-ray spectrometer (EDS mapping). Nexus FTIR Spectrophotometer and INVIA spectrophotometer were applied to detect FTIR and Raman spectra, respectively. To abtain UV-Vis absorption spectra, a UV-2450 spectrophotometer was employed. The XPS data was carried out with a KRATOA XSAM800 system. The Zeta potentials were determined using a Malvern Zetasizer ZEN 3600 analyzer (Malvern Instruments Ltd., Malvern, U.K.). The XPS valence-band spectra measurements were carried out on a ThermoFisher EscaLab 250Xi at a 01 angle of emission using a monochromatic Al Ka source (E_{photon} = 1486.6 eV) with a 10 mA filament current and a 14.7 keV filament voltage source energy. The above measurements were carried out in a field of 0.5 mm and a pass energy of 30 eV. In order to compensate for the charging of the sample, a charge neutralizer was used.

1.5 Photoelectrochemical Measurements

The photoelectrochemical tests, including transient photocurrent responses (*J-t* curve) and electrochemical impedance spectroscopy (EIS), were performed on a CHI660E workstation during a nitrogen atmosphere using the sulfur-rich solution. The photocatalyst-coated FTO, Ag/AgCl and Pt wire works as the working, reference and counter electrode, respectively. The working electrode was prepared as follows: photocatalyst powder (20 mg) was dispersed into 2 mL of absolute alcohol, and then, 2 mL of 1 wt % Nafion ethanol mixing solution was added. After ultrasonicated for 10 min, the above suspension was coated on the FTO surface (the effective area was controlled to 1 cm^2) to obtain the photocatalyst-coated FTO electrode. During *J-t* curve measurements, a 420 nm LED (3 W) was used as the light source, and the open-circuit voltage was used as the applied bias. For the EIS measurements, the frequency was applied from 0.001 to 106 Hz with an amplitude of 0.01 V.

1.6 Measurement of apparent quantum efficiency

The apparent quantum efficiency (AQE) of the prepared photocatalysts is calculated via the following equation:

$$AQE(\%) = \frac{number\ of\ reacted\ electrons}{number\ of\ incident\ photons} \times 100\%$$

$$= \frac{number\ of\ evolved\ H2\ molecules\ \times\ 2}{number\ of\ incident\ photons} \times 100\%$$

In this work, the measured power of the 350-W Xe lamp with a UV cutoff filter ($\lambda \geq 420$ nm) and the average power of the LED light (four 3-W 365 nm) was 120, 24.3 mW/cm^2, respectively. Hence, the AQE of the colloidal CdS-NCs and the colloidal $Cd_{0.4}Zn_{0.6}S$-NCs can be calculated to be 52.8, 66.4%, respectively.

1.7 Calculation of the bandgap structure of the colloidal CdZnS-NCs

To get a deeper insight for bandgap structure of the colloidal CdZnS nanocrystals, the position of valence band (VB) and conduction band (CB) are calculated using the following equations, which is similar to the previous works [1, 2, 3]. $Cd_xZn_yS_z$ was taken as an example for the following equations:

$$E_{VB} = X - E^e + 1/2E_g$$

$$E_{CB} = X - E^e - 1/2E_g$$

$$X = \{X_{Zn}{}^x \times X_{Cd}{}^y \times X_S{}^z\}^{1/(x+y+z)}$$

where X is the absolute electronegativity of CdZnS and E^e is a constant as 4.5 eV. As for X_{Zn}, X_{Cd} and X_S, they are the electronegativities of Zn, Cd and S elements, respectively. Based on the above equations and the obtained E_g values from UV-vis spectra, the conduction band position and valence band position of various colloidal CdZnS nanocrystals could be calculated, and the results were shown in Fig. 4E.

Part II: Supplementary Results

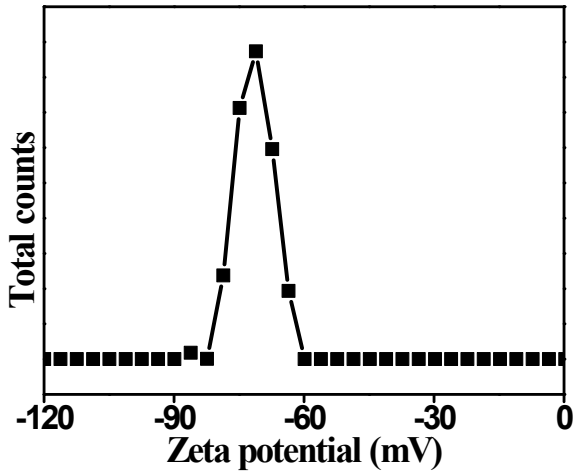

Fig. S1 Zeta potential of the colloidal CdS-NCs solution. The average value of the Zeta potential for the colloidal CdS-NCs solution was measured as -73.5 mV.

Obviously, the colloidal CdS nanocrystals display a very negative potential (-73.5 mV), suggesting its good water solubility, dispersibility, and stability, which can be ascribed to the massive S^{2-} adsorption on the colloidal CdS nanocrystal surface. Usually, the larger the absolute value of Zeta potential, the better the stability of the nanocrystals in water. Therefore, the above results further suggest that the as-synthesized colloidal CdS nanocrystals show an excellent solubility in the sulfur-rich system due to the massive S^{2-} adsorption on its surface. The formation mechanism of the colloidal CdS nanocrystals with massive S^{2-}-adsorption can be described as the following equations:

$$Cd(NO_3)_2 + Na_2S \rightarrow CdS(s) + 2NaNO_3 \qquad \text{eq. (1)}$$

$$CdS(s) + xS^{2-} \rightarrow CdS \bullet xS^{2-} \qquad \text{eq. (2)}$$

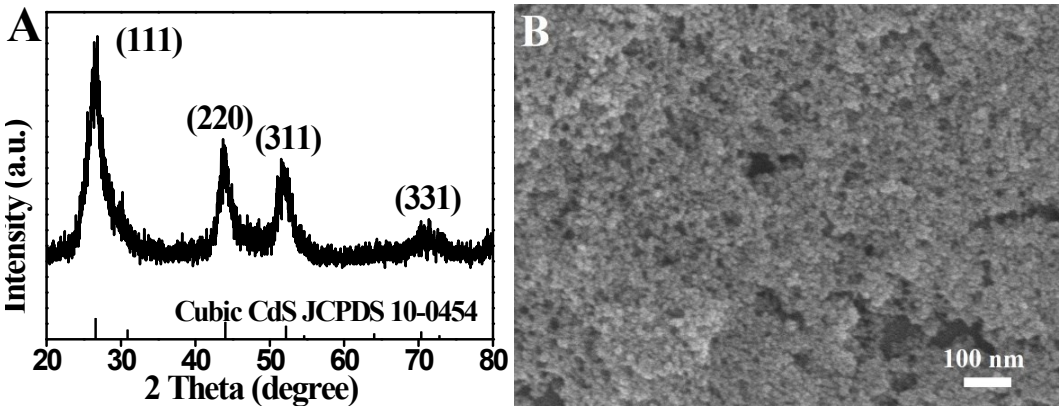

Fig. S2 (A) Powder XRD pattern and (B) SEM image of the colloidal CdS-NCs.

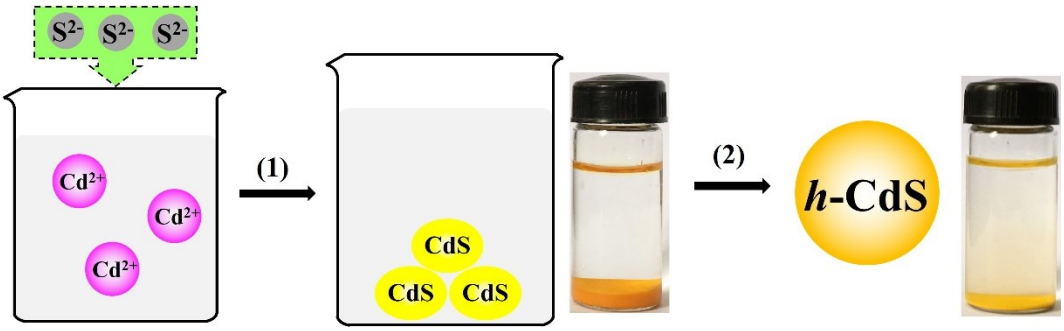

Fig. S3 Traditional precipitation-calcination preparation of hexagonal CdS: step (1) is the formation of cubic CdS precipitation (*c*-CdS); step (2) is the phase transformation to form traditional hexagonal CdS at 550 °C (*h*-CdS).

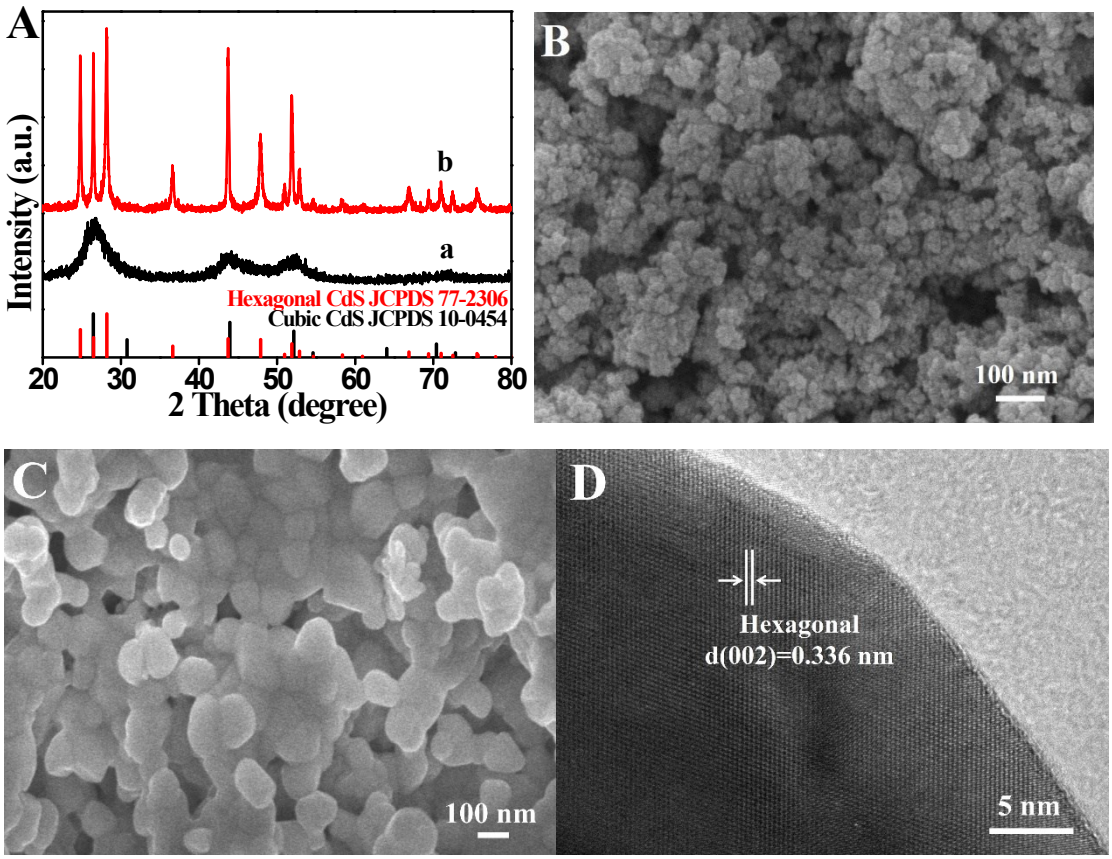

Fig. S4 (A) Powder XRD patterns of (a) *c*-CdS and (b) *h*-CdS. (B, C) FESEM images of (B) *c*-CdS and (C) *h*-CdS. (D) Typical HRTEM image for the *h*-CdS.

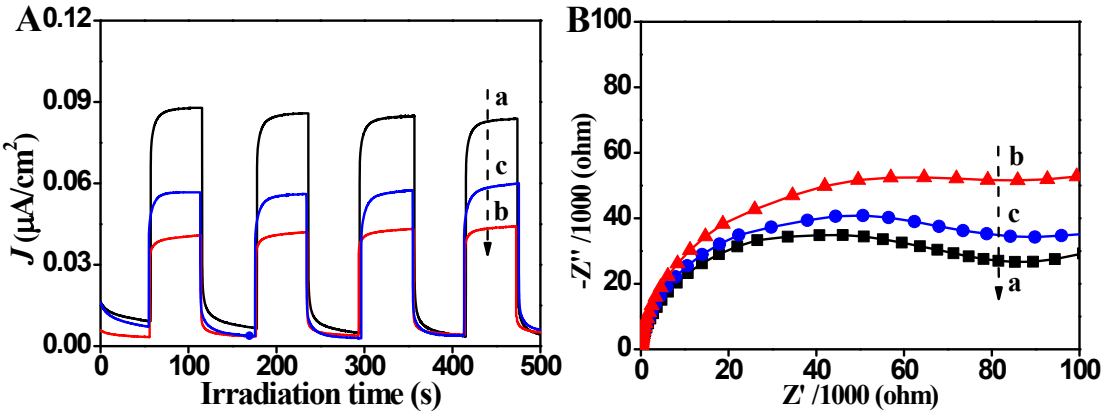

Fig. S5 (A) Transient photocurrent responses (*J*-*t* curve) and (B) electrochemical impedance spectroscopy (EIS) of (a) colloidal CdS-NCs, (b) conventional *c*-CdS and (c) conventional *h*-CdS.

As displayed in Fig. S5A, the colloidal CdS-NCs (Fig. S5A-a) exhibit an increased photocurrent density compared with the conventional *c*-CdS (Fig. S5A-b) and *h*-CdS (Fig. S5A-c) sample, indicating that the photogenerated holes in the colloidal CdS-NCs electrode can be more effectively captured by the S^{2-} than that of the conventional *c*-CdS and *h*-CdS sample, causing a rapider interfacial catalytic reaction. Moreover, the colloidal CdS-NCs sample (Fig. S5B-a) shows a smaller arc radius in the EIS plot than the traditional *c*-CdS (Fig. S5B-b) and *h*-CdS (Fig. S5B-c), revealing a higher transfer efficiency of photogenerated carriers in the colloidal CdS-NCs photocatalyst. Obviously, the above results are in good agreement with their corresponding photocatalytic H_2-evolution performance, and further support the proposed S^{2-}-mediated mechanism for the colloidal CdS-NCs photocatalyst.

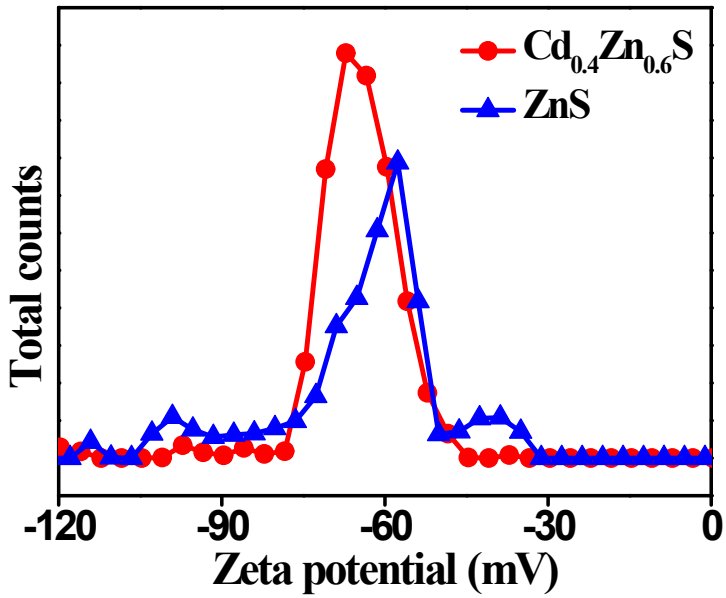

Fig. S6 Zeta potential of the colloidal $Cd_{0.4}Zn_{0.6}S$-NCs and ZnS-NCs solution.

The average value of the Zeta potential for the colloidal $Cd_{0.4}Zn_{0.6}S$-NCs and ZnS-NCs solution was measured as -69.1 and -61.7 mV, respectively, which is mainly attributed to the massive adsorption of S^{2-} and SO_3^{2-}. In this case, the massive adsorption of S^{2-} and SO_3^{2-} on the $Cd_{0.4}Zn_{0.6}S$-NCs and ZnS-NCs can contribute to the excellent stability of colloidal nanocrystals.

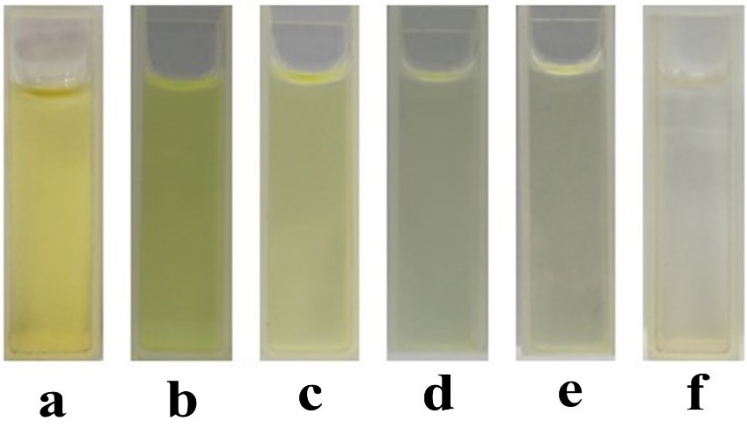

Fig. S7 The optical pictures for the colloidal CdZnS-NC solution: (a) CdS-NCs, (b) $Cd_{0.8}Zn_{0.2}S$-NCs, (c) $Cd_{0.6}Zn_{0.4}S$-NCs, (d) $Cd_{0.4}Zn_{0.6}S$-NCs, (e) $Cd_{0.2}Zn_{0.8}S$-NCs and (f) ZnS-NCs.

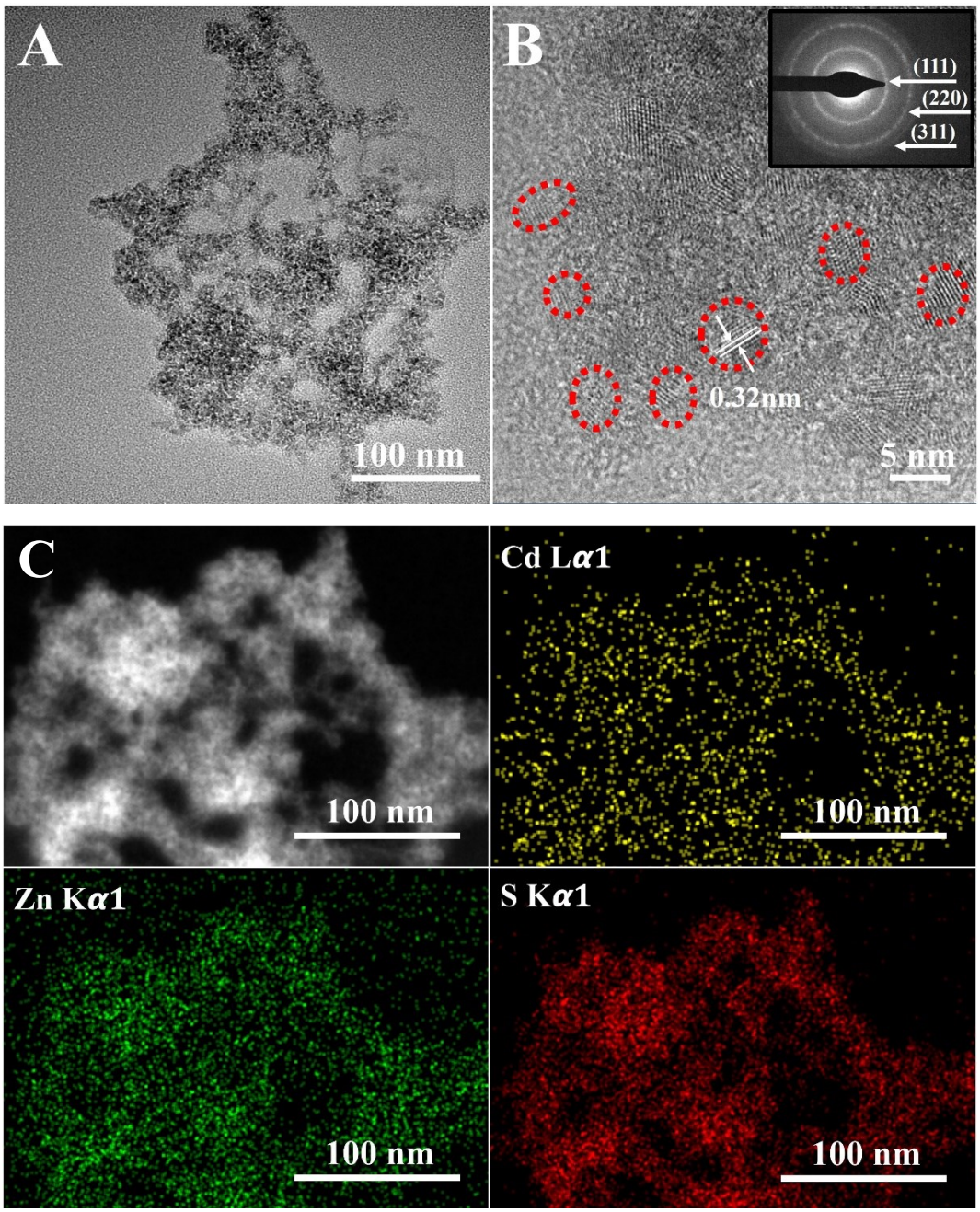

Fig. S8 (A, B) Typical HRTEM images (SAED patterns) and (C) EDS mapping of the colloidal $Cd_{0.4}Zn_{0.6}S$-NCs.

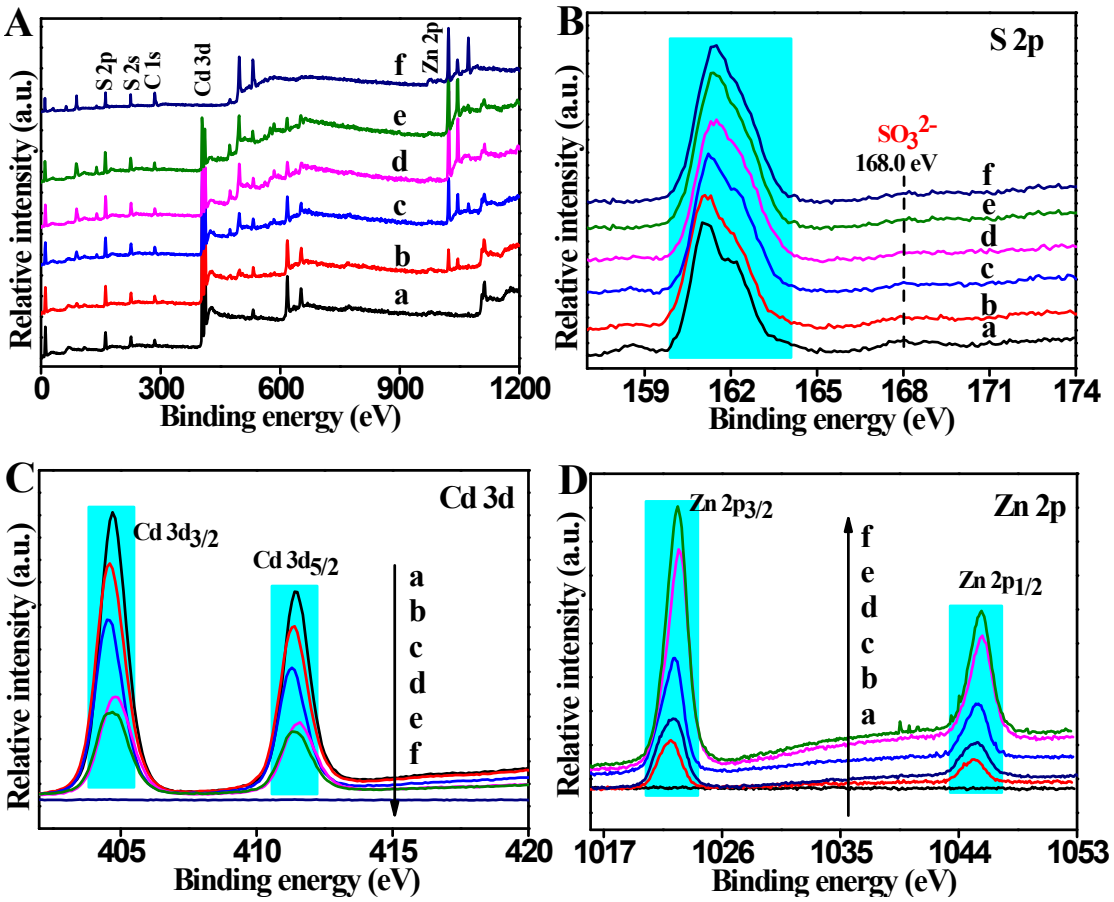

Fig. S9 (A) XPS survey spectra and high-resolution XPS spectra of (B) S 2p, (C) Cd 3d, and (D) Zn 2p for the colloidal CdZnS-NCs: (a) CdS-NCs, (b) $Cd_{0.8}Zn_{0.2}S$-NCs, (c) $Cd_{0.6}Zn_{0.4}S$-NCs, (d) $Cd_{0.4}Zn_{0.6}S$-NCs, (e) $Cd_{0.2}Zn_{0.8}S$-NCs and (f) ZnS-NCs.

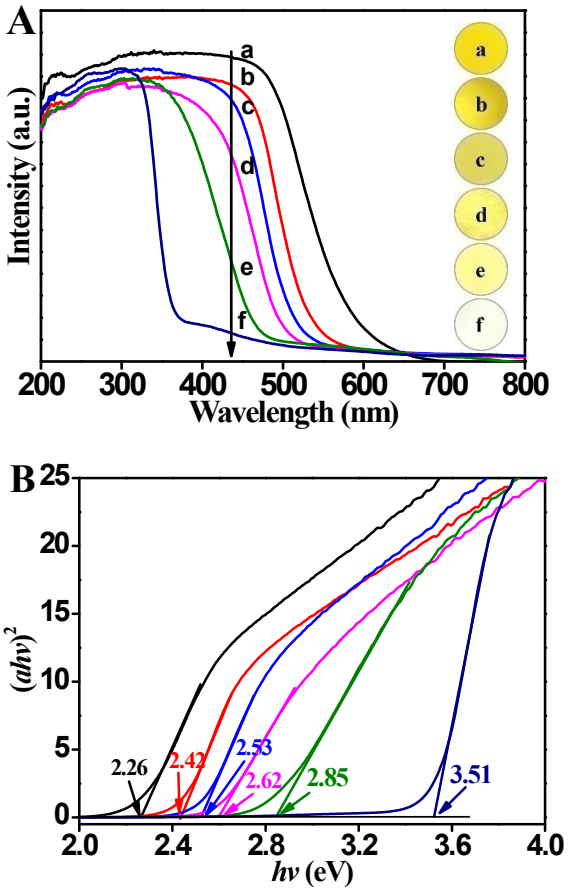

Fig. S10 (A) UV-Vis absorption spectra and (B) band-gap evaluation from the plots for the colloidal CdZnS-NCs: (a) CdS-NCs, (b) $Cd_{0.8}Zn_{0.2}S$-NCs, (c) $Cd_{0.6}Zn_{0.4}S$-NCs, (d) $Cd_{0.4}Zn_{0.6}S$-NCs, (e) $Cd_{0.2}Zn_{0.8}S$-NCs and (f) ZnS-NCs.

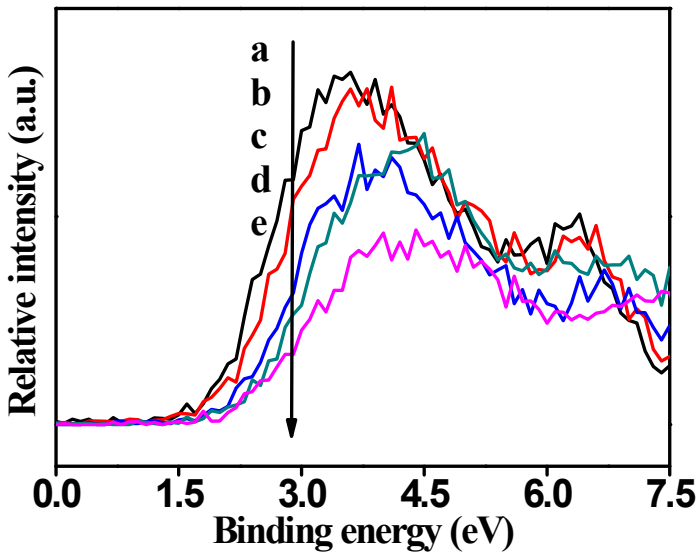

Fig. S11 The XPS valence-band spectra for the colloidal CdZnS-NCs: (a) CdS-NCs, (b) $Cd_{0.8}Zn_{0.2}S$-NCs, (c) $Cd_{0.4}Zn_{0.6}S$-NCs, (d) $Cd_{0.2}Zn_{0.8}S$-NCs and (e) ZnS-NCs.

The XPS valence band spectra of the samples have been performed to further investigate the tunable bandgap for the prepared colloidal CdZnS-NCs. As provided in Fig. S11, the colloidal CdS-NCs exhibit a valence-band position at ca. 1.69 eV, while the colloidal ZnS-NCs possess a more positive valence-band value of ca. 2.33 eV. With increasing Zn content in colloidal CdZnS-NCs, the valence-band position of the colloidal CdZnS-NCs displays a gradual shift from 1.69 to 2.33 eV, strongly demonstrating a controllable bandgap structure of the colloidal CdZnS-NCs. Therefore, the colloidal CdZnS-NCs with a controllable bandgap structure can be easily synthesized via the present facile synthesis method.

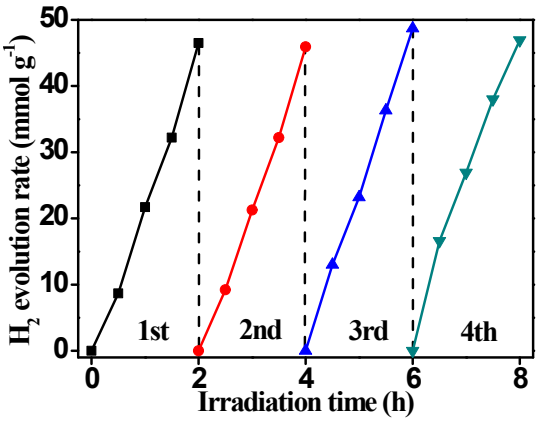

Fig. S12 Cycling runs for the photocatalytic H_2 generation of the colloidal $Cd_{0.4}Zn_{0.6}S$-NC photocatalysts.

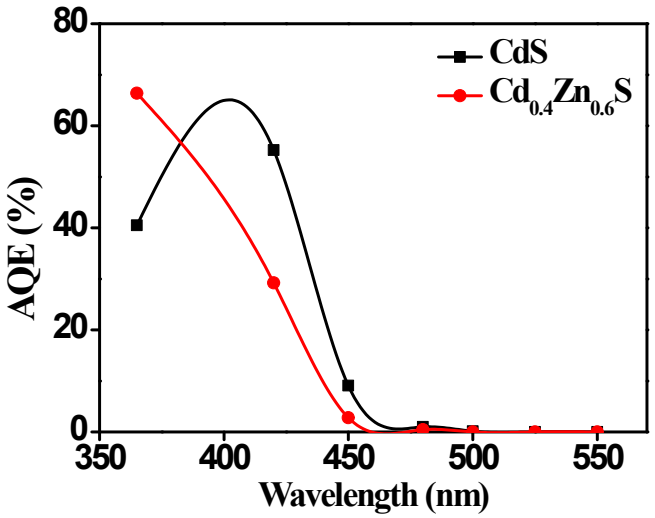

Fig. S13 The wavelength dependent AQE values of the synthesized colloidal CdS-NCs and $Cd_{0.4}Zn_{0.6}S$-NCs photocatalysts.

As displayed in Fig. S13, the colloidal CdS-NCs show extremely low AQE value in the wavelength range over 480 nm, while the colloidal $Cd_{0.4}Zn_{0.6}S$-NCs exhibit an ignorable photocatalytic activity over 460 nm. Clearly, the trends in the wavelength-dependent AQE of the synthesized colloidal CdS-NCs and $Cd_{0.4}Zn_{0.6}S$-NCs closely followed those of the absorbance measured by UV-vis spectra. As demonstrated in Fig. S10, there is a gradual blue shift of the absorption edges by introducing and increasing Zn content in the colloidal CdS-NCs, resulting in a decreased light-absorption property of the colloidal $Cd_{0.4}Zn_{0.6}S$-NCs in visible-light region. Therefore, in comparison with the colloidal CdS-NCs, the decreased photocatalytic activity of the colloidal $Cd_{0.4}Zn_{0.6}S$-NCs in the visible-light region can be ascribed to its weakened visible-light-absorption ability.

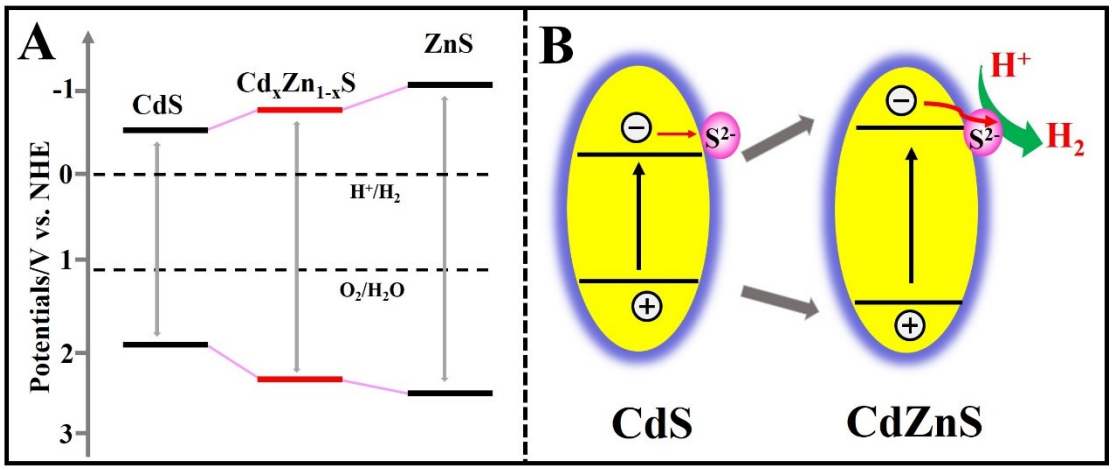

Fig. S14 (A) The band structures of the colloidal CdZnS-NCs and (B) the comparison of the photocatalytic mechanism of the colloidal CdS-NC and the colloidal CdZnS-NC photocatalysts.

Table S1 Comparison of the photocatalytic H_2-evolution rates for typical cocatalyst-modified CdS photocatalysts.

Photocatalyst	Light source	Sacrificial agent	Cocatalyst	Activity [mmol·h^{-1} g^{-1}]	AQE [%]	Ref.
Colloidal CdS-NCs	350 W Xe (> 420 nm)	S^{2-}/SO_3^{2-}	**None**	**6.86**	**52.8**	**This work**
CdS/Au-SCN	350 W Xe (> 420 nm)	S^{2-}/SO_3^{2-}	Au, SCN^-	2.19	11.25	[1]
CdS/GNR	300 W Xe (> 420 nm)	Lactic acid	GNRs	1.89	19.3	[2]
Cd/CdS	300 W Xe (> 420 nm)	S^{2-}/SO_3^{2-}	Cd	0.77	0.82	[3]
CdS/GQDs	300 W Xe (> 420 nm)	S^{2-}/SO_3^{2-}	GQDs	2.39	4.2	[4]
CdS/Au-Co	350 W Xe (> 420 nm)	Lactic acid	Au, Co^{2+}	1.73	-	[5]
MoS_2/CdS	300 W Xe (> 420 nm)	Lactic acid	MoS_2	3.14	3.66	[6]
CoP/CdS/rGO	300 W Xe (> 420 nm)	Lactic acid	CoP, rGO	1.10	-	[7]
CdS/g-C_3N_4	300 W Xe (> 420 nm)	Lactic acid	Pt	2.54	-	[8]
NiS/CdS	300 W Xe (> 420 nm)	Lignin, Lactic acid	NiS	1.51	44.9	[9]
CdS/WS_2/GO	500 W Xe (> 420 nm)	S^{2-}/SO_3^{2-}	WS_2, GO	1.84	21.2	[10]

References

[1] P. Wang, Y. Sheng, F. Wang and H. Yu, *Appl. Catal., B,* 2018, **220**, 561-569.

[2] Y. Xia, B. Cheng, J. Fan, J. Yu and G. Liu, *Small,* 2019, **15**, 1902459.

[3] W. Zhong, S. Shen, M. He, D. Wang, Z. Wang, Z. Lin, W. Tu and J. Yu, *Appl. Catal., B,* 2019, **258**, 117967.

[4] Y. Lei, C. Yang, J. Hou, F. Wang, S. Min, X. Ma, Z. Jin, J. Xu, G. Lu and K. Huang, *Appl. Catal., B,* 2017, **216**, 59-69.

[5] X. Yi, H. Li, P. Wang, J. Fan and H. Yu, *Appl. Surf. Sci.,* 2019, **473**, 144786.

[6] Z. Zhang, Q. Li, X. Qiao, D. Hou and D. Li, *Chin. J. Catal.,* 2019, **40**, 371-379.

[7] H. An, X. Yan, H. Li, B. Yang, J. Wei and G. Yang, *ACS Appl. Energy Mater.,* 2019, **2**, 4195-4204.

[8] L. Chen, Y. Xu and B. Chen, *Appl. Catal., B,* 2019, **256**, 117848.

[9] C. Li, H. Wang, S. Naghadeh, J. Zhang and P. Fang, *Appl. Catal., B,* 2018, **227**, 229-239.

[10]Q. Xiang, F. Cheng and D. Lang, *ChemSusChem,* 2016, **9**, 996-1002.